Bulletin of the Chemical Society of Japan, 2024, **97**, uoad022
https://doi.org/10.1093/bulcsj/uoad022
Advance access publication 26 December 2023

Articles

Improved synthesis of free bases of 5,10,15,20-tetraaryl-5,15-diazaporphyrinoid for conversion to silicon(IV) complexes

Hiroya Suzuki[1], Ko Furukawa[2], Mao Minoura[3], Haruyuki Nakano[4], Yoshihiro Matano[5,*]

[1]Department of Fundamental Sciences, Graduate School of Science and Technology, Niigata University, Ikarashi 8050, Nishi-ku, Niigata 950-2181, Japan
[2]Center for Coordination of Research Facilities, Institute for Research Administration, Niigata University, Ikarashi 8050, Nishi-ku, Niigata 950-2181, Japan
[3]Department of Chemistry, College of Science, Rikkyo University, Nishiikebukuro 3-34-1, Toshima-ku, Tokyo 171-8501, Japan
[4]Department of Chemistry, Graduate School of Science, Kyushu University, 744 Motooka, Nishi-ku, Fukuoka 819-0395, Japan
[5]Department of Chemistry, Faculty of Science, Niigata University, Ikarashi 8050, Nishi-ku, Niigata 950-2181, Japan
*Corresponding author: Department of Chemistry, Faculty of Science, Niigata University, Ikarashi 8050, Nishi-ku, Niigata 950-2181, Japan.
Email: matano@chem.sc.niigata-u.ac.jp

Hiroya Suzuki graduated from Niigata University in 2023 and is currently a graduate student at the same university.

Abstract

We report herein an improved method for the quantitative preparation of free bases of 5,10,15,20-tetraaryl-5,15-diazaporphyrinoid (TADAP) using Me_3SiBr–MeOH to treat the corresponding zinc(II) complexes. Metallation of the free base with $HSiCl_3$ followed by Si–X metathesis with SbF_3 and redox reactions afforded difluorosilicon(IV) complexes of TADAP.

Keywords: diazaporphyrin, free base, silicon(IV) complex.

Graphical Abstract

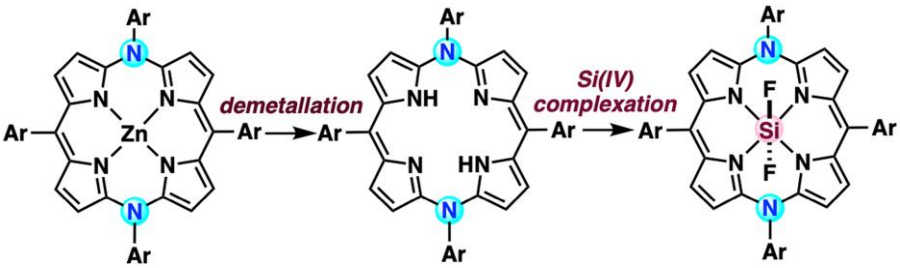

Free bases of 5,10,15,20-tetraaryl-5,15-diazaporphyrinoid (TADAP) were easily prepared using Me_3SiBr–MeOH to treat the corresponding zinc(II) complexes. The first examples of difluorosilicon(IV) complexes of TADAP were successfully prepared from the free base and trichlorosilane.

1. Introduction

Porphyrins are well-known redox-active 18π-electron aromatic molecules, and their oxidized/reduced species have attracted considerable attention because they are involved in various phenomena, including electron/energy-transfer processes, semiconduction, and aromaticity–antiaromaticity switching.[1] However, 19π-electron radical anions and 20π-electron dianions of porphyrin are extremely unstable in air, making isolation and characterization of these anionic species difficult. Several research groups have developed charge-shifting methods to stabilize 19π- and 20π-electron porphyrins, which can

[Received on 25 October 2023; revised on 4 December 2023; accepted on 16 December 2023; corrected and typeset on 26 February 2024]

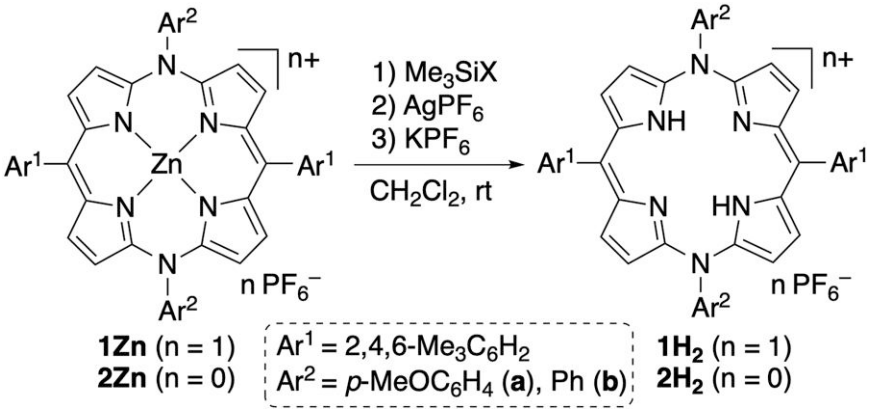

Scheme 1. Synthesis of TADAP free bases.

then be isolated in the uncharged state.[2–8] Recently, we prepared the first examples of metal complexes of 5,10,15,20-tetraaryl-5,15-diazaporphyrinoid (MTADAP; M = Co, Ni, Cu, Zn) by metal-templated annulation of the corresponding metal(II)–bis(dipyrrin) complexes.[9–11] Notably, most MTADAPs in the 20π- and 19π-electron forms are stable in air and exhibit characteristic optical, magnetic, and electrochemical properties depending on the central metal. However, the metal-templated annulation method is currently applicable only to the above four metals. Therefore, it is important to develop a general protocol for the metal complexation of free bases of TADAP (H_2TADAP). In our previous work, H_2TADAPs were obtained in moderate yields by demetallation of the corresponding ZnTADAPs, referring to the Yorimitsu–Osuka protocol for the synthesis of porphyrins.[12] Unfortunately, this method requires large excess amounts of a Grignard reagent and trifluoroacetic acid, sometimes contaminating the reaction system with byproducts. In this study, we developed a more convenient and reproducible protocol to obtain H_2TADAP. The structure, aromaticity, and optical and redox properties of the newly prepared silicon(IV) complexes of TADAP were also revealed.

2. Results and discussion

ZnTADAPs **1Zn-a** and **2Zn-a,b** were prepared according to the previously-reported method.[10] Scheme 1 and Table 1 summarize the results of reacting **1Zn-a** and **2Zn-a,b** with several acids. The reactions were monitored using high-resolution mass (HRMS) spectrometry and ultraviolet/visible/near-infrared (UV/vis/NIR) absorption spectroscopy. When **1Zn-a** was treated with aqueous solutions of HCl, HBr, and H_2SO_4 in CH_2Cl_2 at room temperature, demetallation did not occur (Table 1, entries 1 to 3). By contrast, when trimethylsilyl halides (Me_3SiX; X = Cl, Br, I) were used instead of HX aq, demetallation of **1Zn-a** took place to generate desired H_2TADAP **1H$_2$-a** together with inseparable byproducts (entries 4 to 6; The ^{1}H NMR and HRMS data suggested that small amounts of halogenated TADAPs were included, although their structures could not be identified. These byproducts may be formed via nucleophilic attack of the halide ions onto the cationic TADAP ring). Moreover, Me_3SiOTf was ineffective in promoting demetallation (entry 7). When **2Zn-a** was used as the substrate, formation of the byproducts was completely suppressed and high-purity **1H$_2$-a** was obtained (entries 8, 9). Furthermore, the yield of **1H$_2$-a** was improved by adding appropriate amounts of MeOH (entries 10, 11). Similarly, **2Zn-b** was demetallated with Me_3SiBr–MeOH to yield **1H$_2$-b** (entry 12).

Table 1. Results for demetallation of ZnTADAPs.

Entry	1/2	Acids (equiv.)	Time (h)	Yield (%)[a,b]
1	**1Zn-a**	HCl aq[c]	2	N.r.
2	**1Zn-a**	HBr aq[d]	2	N.r.
3	**1Zn-a**	H_2SO_4 aq[e]	2	N.r.
4	**1Zn-a**	Me_3SiCl (70)	32	ca.50[f]
5	**1Zn-a**	Me_3SiBr (5)	3	ca.80[f]
6	**1Zn-a**	Me_3SiI (5)	3	ca.50[f]
7	**1Zn-a**	Me_3SiOTf (5)	76	N.r.
8	**2Zn-a**	Me_3SiCl (70)	18	60
9	**2Zn-a**	Me_3SiBr (20)	5	75
10	**2Zn-a**	Me_3SiBr–MeOH (30)	5	98[g]
11	**2Zn-a**	Me_3SiCl–MeOH (70)	5	74
12	**2Zn-b**	Me_3SiBr–MeOH (30)	12	82[g]

[a]N.r., No reaction.
[b]NMR yields of **2H$_2$**, which were obtained by treatment of the product mixtures including **1H$_2$** with $CoCp_2$, are listed unless otherwise noted.
[c]ca. 35%.
[d]ca. 50%.
[e]ca. 95%.
[f]Unidentified byproducts were formed.
[g]Isolated yields of **1H$_2$**.

The above demetallation of ZnTADAP with Me_3SiX–MeOH (X = Cl, Br) likely proceeded as follows. The HX molecule, generated in situ from Me_3SiX and MeOH, strongly interacts with the Zn–N bond via axial coordination of the halide ion to the zinc center of **2Zn**. Subsequently or simultaneously, the internal N atom of **2Zn** is protonated to release the zinc ion via metathesis. In the absence of MeOH, the trace amount of water remaining in the solvent might facilitate the hydrolysis of Me_3SiX to generate HX (entries 4 to 9). In HX aq solutions, the counter anions are likely solvated by water molecules and cannot effectively coordinate to the zinc center (entries 1 to 3). Unsuccessful demetallation by Me_3SiOTf indicated that coordination of the triflate ion was insufficient to enhance the reactivity of the Zn–N bond toward protons. The optimized synthesis procedure is described in section 4.

With the TADAP free bases in hand, complexation of **2H$_2$-a** with the silicon(IV) ion using Adler's method was examined (Scheme 2).[13] Treatment of **2H$_2$-a** with $HSiCl_3$ in CH_2Cl_2 at room temperature afforded an inseparable mixture of silicon(IV) complexes of TADAP with different axial ligands. ^{1}H NMR and HRMS data of the crude product suggested that the axial ligands were hydroxy and/or chloride ions. To isolate

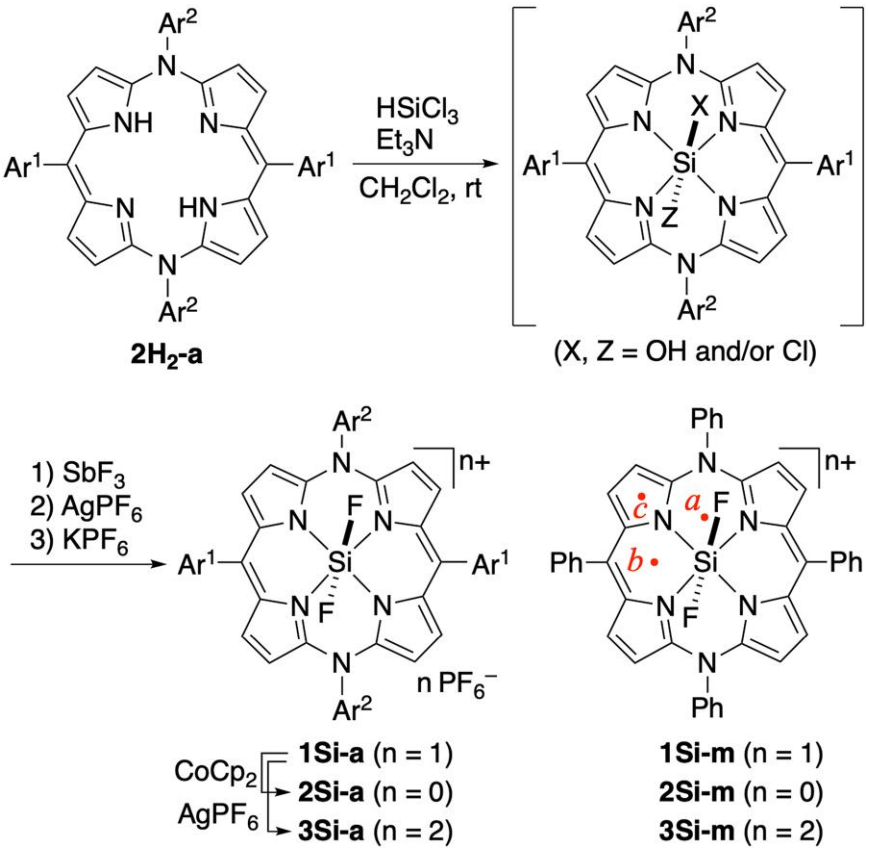

Scheme 2. Synthesis of SiF_2TADAP.

a single silicon(IV) complex, the resulting mixture was reacted with SbF_3 to convert all axial ligands to fluoride ions and then treated with $AgPF_6$ to convert the TADAP ligand to the 19π-electron state. Finally, SiF_2TADAP radical cation **1Si-a** was isolated using silica-gel column chromatography. Reduction of **1Si-a** with cobaltocene ($CoCp_2$) in THF yielded high-purity SiF_2TADAP **2Si-a** in the 20π-electron state, which was confirmed with ^{1}H and ^{19}F{^{1}H} NMR spectra. **2Si-a** was found to be stable to hydrolysis and methanolysis. Oxidation of **1Si-a** with $AgPF_6$ in CD_2Cl_2 quantitatively produced SiF_2TADAP dication **3Si-a** (vide infra). However, **3Si-a** could not be isolated because it readily reduced to the 19π-electron species under ambient conditions.

The crystal structure of **1Si-a** (CCDC Deposition Number: 2303271) is depicted in Fig. 1. The silicon center has an octahedral geometry with Si–N and Si–F bond lengths of 1.9347(15) to 1.9415(16) and 1.6292(11) Å, respectively. The Si–N bonds in **1Si-a** are slightly longer than those in the difluorosilicon(IV) complexes of 5,10,15,20-tetraarylporphyrins (aryl = *p*-tolyl, *p*-$CF_3C_6H_4$).[14] It is worth noting that **1Si-a** has a highly flat DAP ring with a root mean square deviation of 0.043 Å (Supplementary Fig. S1).

Figure 2 shows the ^{1}H NMR spectra of **2Si-a** and **3Si-a**. The pyrrolic-β protons of **2Si-a** in C_6D_6 gave rise to peaks at 4.66 and 3.32 ppm, whereas those of **3Si-a** in CD_2Cl_2 gave rise to peaks at 9.07 and 8.80 ppm. These widely separated upfield and downfield shifts indicated the presence of substantial paratropic (20π) and diatropic (18π) ring currents, respectively. In the ^{19}F NMR spectra of **2Si-a** and **3Si-a**, the axial fluorine signal appeared at −68.3 and −114.1 ppm (vs. $CFCl_3$), respectively. Similarly, these upfield and downfield shifts reflected the effects of paratropic and diatropic ring currents, respectively. Therefore, the DAP rings of **2Si-a** and **3Si-a** exhibited antiaromaticity and aromaticity, respectively. The axial fluorine atoms of **3Si-a** were slightly less shielded than those of the difluorosilicon(IV) complex of 5,10,15,20-tetraphenylporphyrin (SiF_2TPP; $\delta_F = -121.4$ ppm vs. $CFCl_3$),[15] which indicated that the diatropic ring-current effect of the DAP ring in **3Si-a** was slightly weaker than that of the porphyrin ring in SiF_2TPP. In the ^{29}Si NMR spectrum of **2Si-a**, a triplet signal appeared at −183.0 ppm (vs. TMS; $J_{Si-F} = 197$ Hz). The ^{29}Si resonance of **2Si-a** is shifted upfield by 90 ppm compared to that of antiaromatic Si(TPP)$(py)_2$ (−93 ppm),[3] which may reflect the large difference in the electronic effects of the axial ligands (py = pyridine).

To gain insight into the ring-current effects of the TADAP and TPP π-electron systems, we calculated the nuclear independent chemical shift (NICS) at three/two positions in the π-planes of **2Si-m**, **3Si-m**, and SiF_2TPP, which were structurally optimized using the density functional theory (DFT) method (Supplementary Table S1 and Fig. S2). Owing to the paratropic ring current of the 20π-electron DAP ring, the calculated NICS(0) values at the *a* and *b* positions of **2Si-m** were +6.82 and +7.09 ppm, respectively. The calculated NICS(0) values at the same *a* and *b* positions of **3Si-m** were −17.20 and −17.65 ppm, respectively, which were less negative than the corresponding value (−18.18 ppm) at the *a* position of SiF_2TPP. This indicated that the macrocyclic diatropic ring-current effect of the 18π SiF_2TADAP dication was slightly weaker than that of isoelectronic SiF_2TPP. This difference was attributed to the different current densities of these two 18π-electron systems. Furthermore, we calculated the

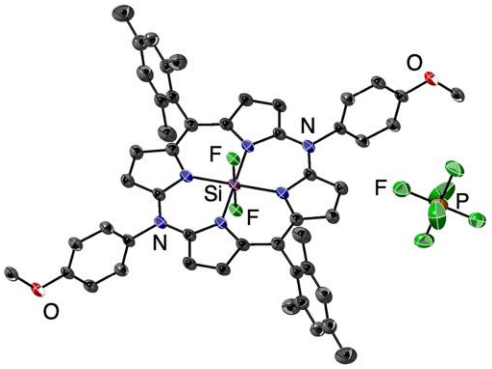

Bond lengths (Å)	
Si–N	1.9347(15)–1.9415(16)
Si–F	1.6292(11)
N_{meso}–C_{α}	1.354(2)–1.355(2)
C_{meso}–C_{α}	1.378(3)–1.382(3)

Fig. 1. ORTEP diagram (50% probability ellipsoids) and bond lengths of **1Si-a**. Hydrogen atoms are omitted for clarity.

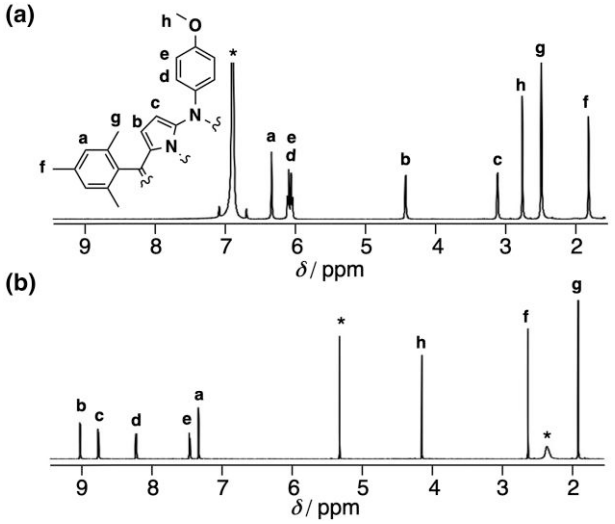

Fig. 2. ^{1}H NMR spectra of a) **2Si-a** in C_6D_6 and b) **3Si-a** in CD_2Cl_2. Asterisks indicate residual solvent peaks.

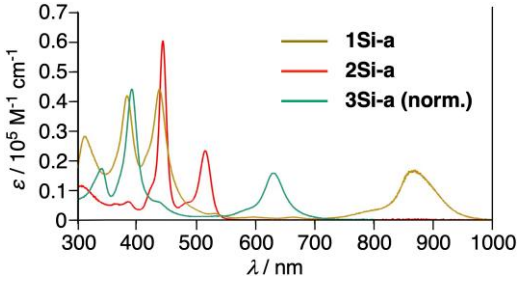

Fig. 3. UV/vis/NIR absorption spectra of SiF_2TADAPs in CH_2Cl_2. The spectrum of **3Si-a** was measured in the presence of a small amount of $AgPF_6$ and normalized to that of **1Si-a**.

^{19}F chemical shifts of the three models at the DFT level with gauge-including atomic orbitals (Supplementary Table S2). Although there were discrepancies in the absolute values, the order of the calculated chemical shifts for **2Si-m** (−105.1 ppm), **3Si-m** (−162.8 ppm), and SiF_2TPP (−172.4 ppm) was identical to the order of the observed chemical shifts for the series of **2Si-a**, **3Si-a**, and SiF_2TPP (vide supra). Overall, both the NMR spectra and DFT calculations clarified the antiaromaticity and aromaticity of 20π- and 18π-electron SiF_2TADAPs, respectively.

The ESR spectra of **1Si-a** in CH_2Cl_2 are shown in Supplementary Fig. S3. The hyperfine-coupling structure observed for **1Si-a** as well as spin densities calculated for **1Si-m** revealed that an electron spin of this radical was efficiently delocalized over the entire DAP ring. The lack of hyperfine coupling with silicon and fluorine atoms indicated that the SiF_2 unit in the core simply affected the orbital energies of the TADAP π-radical.

As shown in Fig. 3, the UV/vis/NIR absorption spectra of **1Si-a**, **2Si-a** and **3Si-a** in CH_2Cl_2 contained characteristic absorption bands corresponding to the 19π-, 20π-, and 18π-electronic states of the TADAP skeleton, respectively. To reveal the nature of these π–π* electronic transitions, we carried out time-dependent DFT (TD–DFT) calculations of their models, and the results are summarized in Supplementary Table S3. The Q-like band of **3Si-a** (λ_{max} = 631 nm), corresponding to the HOMO-to-LUMO electronic transition, was significantly red-shifted and intensified compared with the Q band of SiF_2TPP (λ_{max} = 521 nm). This trend was similar to that observed for the other metal(II) complexes (MTADAP vs. MTPP).

The redox potentials of **1Si-a** in CH_2Cl_2 were measured using cyclic voltammetry with Bu_4NPF_6 as the supporting electrolyte (Supplementary Fig. S4). The SiF_2TADAP π-electron system underwent three reversible redox processes at −1.81, −0.29, and +0.44 V vs. ferrocene/ferrocenium (Fc/Fc^+), which were attributed to the 21π/20π, 20π/19π, and 19π/18π redox couples, respectively. These half-wave potentials were shifted toward the more positive side compared with the corresponding potentials of the zinc(II), nickel(II), and copper(II) complexes of the same TADAP ligand,[10] suggesting that SiF_2 functioned as an electron-withdrawing unit. The orbital energies calculated using the DFT method supported this trend. Notably, the SiF_2 unit significantly contributed to stabilizing the antiaromatic 20π-electron state of the DAP ring in air.

3. Conclusion

We developed a new method for the synthesis of free bases of TADAP from the corresponding zinc(II) complexes. Using Me_3SiBr–MeOH improved the previously reported method in terms of reaction efficiency and reproducibility. Furthermore, we successfully converted the free base to the first examples of difluorosilicon(IV) complexes of TADAP and characterized the structures of the complexes using spectroscopic techniques and DFT calculations.

The ring-current effects of the TADAP ligand were investigated using ^{1}H and ^{19}F NMR spectroscopy and NICS calculations, all of which revealed the antiaromaticity and aromaticity of the 20π- and 18π-electron DAP rings, respectively.

4. Experimental

Demetallation of ZnTADAP: **1Zn-a** (158 mg, 163 μmol) was dissolved in THF (5.0 mL) and reduced to **2Zn-a** with $NaBH_4$. After exchanging the solvent from THF to CH_2Cl_2 (4 mL), MeOH and Me_3SiBr (each, 30 equiv.) were added, and the resulting solution was stirred at room temperature for 5 h. As the crude product contained both 19π- and 20π-electron species, $AgPF_6$ was added to the product mixture, followed by treatment with an aqueous KPF_6 solution. The radical cation of free base **$1H_2$-a** was isolated in 98% yield by silica-gel column chromatography. For details, see the online supplementary material.

Supplementary data

Supplementary material is available at *Bulletin of the Chemical Society of Japan* online.

Funding

This work was supported by Japan Society for the Promotion of Science KAKENHI (22H02061 to YM, 21K04980 to HN) from the Ministry of Education, Culture, Sports, Science and Technology, Japan. We would also like to express our gratitude to the SPring-8 synchrotron facility, where synchrotron-radiation experiments were performed at the BL02B1 beamlines with the approval of the Japan Synchrotron Radiation Research Institute (JASRI) under proposal numbers 2022A1200, 2022B1603, 2023B1675, 2023A1727, 2023A1771, and 2023A1925.

Conflict of interest statement. The authors declare no conflict of interest.

References

1. *Handbook of Porphyrin Science*, ed. by K. M. Kadish, K. M. Smith, R. Guilard, World Scientific, Singapore, **2010–2022**, Vols. *1–46*.
2. E. Vogel, M. Pohl, A. Herrmann, T. Wiss, C. König, J. Lex, M. Gross, J. P. Gisselbrecht, *Angew. Chem. Int. Ed. Engl.* **1996**, *35*, 1520.
3. J. A. Cissell, T. P. Vaid, A. L. Rheingold, *J. Am. Chem. Soc.* **2005**, *127*, 12212.
4. J. A. Cissell, T. P. Vaid, G. P. A. Yap, *J. Am. Chem. Soc.* **2007**, *129*, 7841.
5. T. Yoshida, W. Zhou, T. Furuyama, D. B. Leznoff, N. Kobayashi, *J. Am. Chem. Soc.* **2015**, *137*, 9258.
6. S. P. Panchal, S. C. Gadekar, V. G. Anand, *Angew. Chem. Int. Ed.* **2016**, *55*, 7797.
7. Y. Matano, *Chem. Rev.* **2017**, *117*, 3138.
8. Y. Matano, *Org. Biomol. Chem.* **2023**, *21*, 3034, and references therein.
9. T. Satoh, M. Minoura, H. Nakano, K. Furukawa, Y. Matano, *Angew. Chem. Int. Ed.* **2016**, *55*, 2235.
10. K. Sudoh, T. Satoh, T. Amaya, K. Furukawa, M. Minoura, H. Nakano, Y. Matano, *Chem. Eur. J.* **2017**, *23*, 16364.
11. Y. Satoh, Y. Kudoh, K. Furukawa, Y. Matano, *Org. Lett.* **2022**, *24*, 3839.
12. K. Murakami, Y. Yamamoto, H. Yorimitsu, A. Osuka, *Chem. Eur. J.* **2013**, *19*, 9123.
13. B. A. Hussein, Z. Shakeel, A. T. Turley, A. N. Bismillah, K. M. Wolfstadt, J. E. Pia, P. M. Pilkington, P. R. McGonigal, M. J. Adler, *Inorg. Chem.* **2020**, *59*, 13533.
14. K. M. Kane, F. R. Lemke, J. L. Petersen, *Inorg. Chem.* **1997**, *36*, 1354; Si–N bond lengths: 1.911(2)–1.925(2) Å.
15. K. M. Kane, C. R. Lorenz, D. M. Heilman, F. R. Lemke, *Inorg. Chem.* **1998**, *37*, 669. The ^{19}F chemical shift of SiF_2TPP was reported to be −44.5 ppm vs. CF_3CO_2H.